RESEARCH ARTICLE

# Maytansinol Functionalization: Towards Useful Probes for Studying Microtubule Dynamics

Zlata Boiarska,[a]¥ Helena Pérez-Peña,[a]¥ Anne-Catherine Abel,[b]¥ Paola Marzullo,[a]¥ Beatriz Álvarez-Bernad,[c] Francesca Bonato,[c] Benedetta Santini,[a] Dragos Horvath,[d] Daniel Lucena-Agell,[c] Francesca Vasile,[a] Maurizio Sironi,[a] J. Fernando Díaz,[c] Andrea E. Prota,[b] Stefano Pieraccini,*[a] and Daniele Passarella*[a]

[a] Z. Boiarska, H. Pérez-Peña, Dr. P. Marzullo, Dr. B. Santini, Prof. Dr. F. Vasile, Prof. Dr. M. Sironi, Prof. Dr. S. Pieraccini, Prof. Dr. D. Passarella
Department of Chemistry, Università degli Studi di Milano
Via Golgi 19, 20133 Milan (Italy)
E-mail: daniele.passarella@unimi.it
Homepage: https://sites.unimi.it/passalab/

[b] A-C. Abel, Dr. A.E. Prota,
Laboratory of Biomolecular Research, Paul Scherrer Institute
Forschungsstrasse 111, 5232 Villigen PSI (Switzerland)

[c] B. Álvarez-Bernad, F. Bonato, Dr. D. Lucena-Agell, Dr. J. F. Díaz
Centro de Investigaciones Biológicas Margarita Salas
Consejo Superior de Investigaciones Científicas
Ramiro de Maeztu 9
28040 Madrid (Spain)

[c] Dr. D. Horvath
Laboratory of Chemoinformatics, Faculty of Chemistry
University of Strasbourg
67081 Strasbourg (France)

¥ The authors contributed equally

Supporting information for this article is given via a link at the end of the document

**Abstract:** Maytansinoids represent a successful class of natural and semisynthetic tubulin binders, known for their potent cytotoxic activity. Their wider application as cytotoxins and chemical probes to study tubulin dynamics was set back due to the complexity of natural product chemistry. Here we report the synthesis of long-chain derivatives and maytansinoid conjugates. We confirmed that bulky substituents do not impact their high activity and the scaffold's binding mode. These encouraging results open new avenues for the design of new maytansine-based probes.

## Introduction

Maytansinoids continue to excite interest almost after a decade since their discovery as potent antimitotic tubulin binders.[1–3] Their highly efficient mechanism of capping MT-dynamics[4] has led to their successful application in cancer treatment as antibody-drug conjugates (ADCs).[5–7] This success has further prompted their development as targeted cancer therapeutics, e.g. in the form of nanoparticles[8,9] or recently reported immune checkpoint-targeting maytansinoid conjugates.[10] However, the high-affinity of maytansine towards β-tubulin ($K_D$ 6.8 – 14 nM) not only makes it well suited as a cytotoxin, but also derivatives with a similar affinity could be used as molecular probes.[11,12] As of today, effortless generation of maytansine-based molecular probes is hampered by major drawbacks such as the complexity of the natural product scaffold and lack of SAR studies, which could suggest suitable points for attachment of fluorophore tags or radionuclides. Here, we report on both of these aspects: the chemistry of maytansinol (Figure 1, **1**) for the creation of maytansinoid conjugates and the suitability of the C3-position to tolerate bulky substituents without affecting the binding mode. Therefore, we provide a solid basis for in-depth exploration of maytansinoids as molecular probes to study microtubule dynamics.

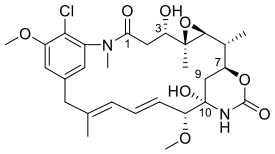


Maytansinol, **1**

**Figure 1.** Chemical structure of maytansinol

Previously, it has been shown that the ester at the C-3 position of ansamitocins, maytansine, and maytansinoids plays an important role in biological activity and cell permeability.[3,13,14] In our recent study, we extensively investigated a series of C-3 derivatized maytansinoids obtained by acylation of maytansinol.[12] By X-ray crystallography experiments, we observed that the studied maytansinoids retained a fundamental spatial arrangement with respect to β-tubulin. The binding mode of the core structure of maytansinol remained unaltered independently of the introduced substituents. Furthermore, the binding affinities of the C3-substituted maytansinoids obtained are very similar to the one of maytansine.

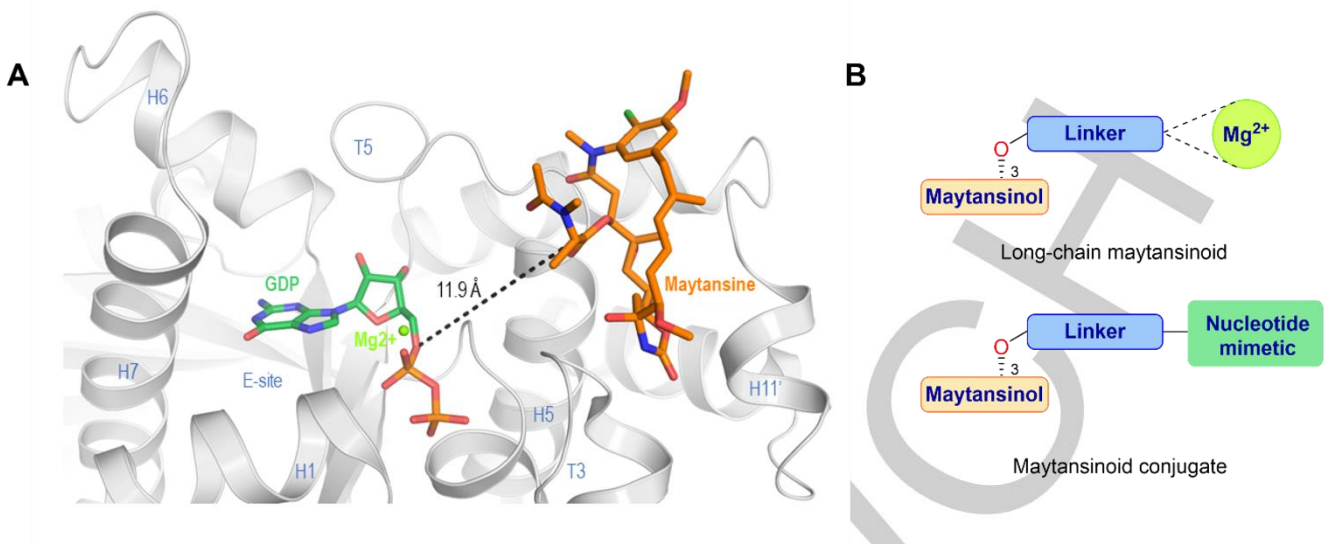


**Figure 2. (A)** Section of the crystal structure with PDB ID 4TV8 in which maytansine (orange), GDP (green), Mg2+ (bright green sphere), and β-tubulin (grey) are present. The black dotted line represents the distance between the C3-position of maytansine and C5-position of the GDP which is ~12Å. **(B)** Schematic drawing of both the maytansinoids and the conjugates designed to target the nucleotide-bound $Mg^{2+}$ or the exchangeable nucleotide site (E-site) of tubulin.

Based on these observations, we decided to further investigate the potential of C-3 functionalized maytansinoids as molecular probes by creating novel tubulin binders. The design of novel maytansinoids was led by the high-resolution X-ray crystallography structures of recently obtained maytansinoid-tubulin complexes (PDB IDs 5SB9, 5SBA and 5SBB). The maytansine binding site is located in proximity of the GDP nucleotide bound to the E-site and a GDP-coordinated $Mg^{2+}$. The first interesting factor that could be exploited to exert a novel effect on MTs is the $Mg^{2+}$ ion coordinated by the nucleotide in close proximity to the maytansine binding site. The design of bivalent compounds containing maytansinol and nucleotide mimetics would *a*) increase the understanding of the ability of maytansinoids to accommodate in the binding site independently of the size of the substituents, and *b*) investigate the ability of these molecules to interact with $Mg^{2+}$ and to displace the nucleotide from the binding site.

Tubulin inhibition by nucleotide analogues is very challenging because of GTP concentrations around 300 μM inside the cells.[15] However, we sought to investigate whether the presence of the maytansinol moiety in a bivalent compound could favor binding of the nucleotide portion through an entropic effect. The maytansinol moiety would act as an anchor point holding the modified nucleotide portion in close proximity of the E-site through a flexible linker, thereby favoring the nucleotide exchange.

Accordingly, we decided to prepare long-chain maytansinol derivatives and maytansinoid conjugates to target either the $Mg^{2+}$ ion or the nucleotide binding site. Introducing different substituents at the 3-*O* position should allow to optimize the protein-ligand interaction and to find new molecules capable of producing different effects on tubulin structure and dynamics.

## Results and Discussion

### ***Design and Synthesis***

**Long-chain maytansinoids**

Initially, we envisioned to obtain the long-chain maytansinoids directly through the acylation reaction of maytansinol, which we previously used for the synthesis of short-chain maytansinoids.[13] To date, neither long-chain maytansinoids of this type nor acylation reaction of maytansinol with a dicarboxylic acid have been reported in the literature. However, initial trials to functionalize maytansinol with a peptide-like linker (**2**) or with a sebacic acid (**3**)**,** using Steglich esterification, were not successful (Scheme 1). This prompted us to change the approach to a two step-synthesis: the preparation of short-chain maytansinoids with a terminal alkene, followed by a cross metathesis (CM) reaction with an unsaturated carboxylic acid. The acylation reaction of maytansinol to obtain **4** and **5** worked well, although lower yields were obtained using longer-chain carboxylic acids. In both cases, the time prolongation had no great influence on the formation of the desired product, and only affected the ratios of different by-products obtained (Scheme 1).

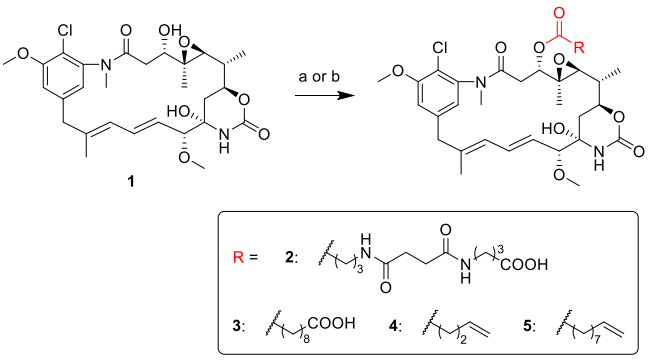


**Scheme 1.** *Reaction conditions*: a) RCOOH 3 equiv., DMAP 3 equiv., DCC 3.3 equiv. in DCM, DCM/DMF 1:1, r.t. or 40°C, 24-48h, **2** n.r. (or **3** n.r.); b) RCOOH 3 equiv., DMAP 3 equiv., DCC 3.3 equiv. in DCM, $ZnCl_2$ 3 equiv., DCM (+10% DMF), 48h, **4** 68% (or **5** 57%).

The preferred length of a long-chain maytansinoid was estimated at 10-11 carbon atoms, based on docking studies. Therefore, compound **5** was then used to obtain the derivative with a desired length **6** through a Ru-catalyzed CM reaction, using

the 2nd generation Hoveyda-Grubbs catalyst. The *trans*-isomer was the one detected by $^1$H NMR analysis (Scheme 2).

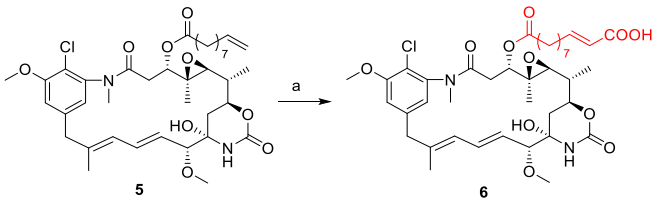


**Scheme 2.** *Reaction conditions*: a) **5** 1 equiv., acrylic acid 2.5 equiv., Hoveyda-Grubbs 2nd gen 20 mol%, DCM, reflux, 18h, **7** 46%.

Importantly, the docking studies showed that the E/Z isomerism did not seem to influence the outcome since both stereo isomers were able to establish the same interactions with the $Mg^{2+}$ even if the poses of the linkers slightly differed from each other (Figure S41).

Obtaining both short-chain maytansinoids **4** and **5** and the long-chain maytansinoid **6** allowed us to perform more studies on maytansinoids SAR based on the length and nature of the chain. Moreover, the long-chain analogue could be exploited to attach other molecules to maytansine.

### Maytansinoid conjugates

We decided to conjugate the maytansinoids with guanosine mimetics and we based the rational linker design on the distance of ~12 Å (Figure 2). In the linker-design stage, the main goal was to define a proper length and flexibility to secure the accommodation of maytansinol and nucleotide-like scaffolds in their respective β-tubulin binding sites.

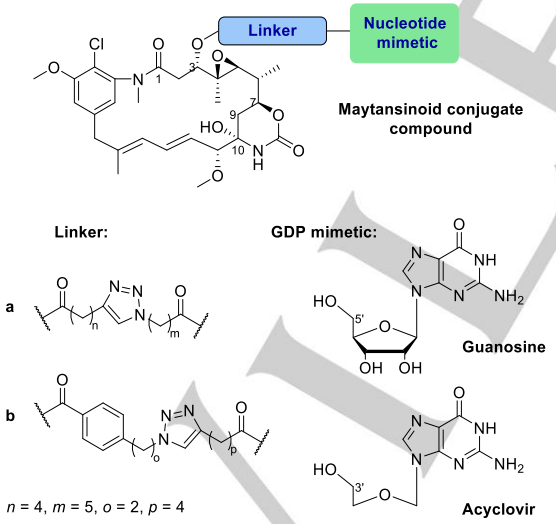


**Figure 3.** Design structures of the maytansinoid-conjugate compounds to target maytansine and GDP binding sites.

First of all, we focused on the linkers which could allow the conjugation of the compounds of interest by means of click chemistry. We generated a library of 54 possible linkers in which the position of the triazole group and the length of the carbon tails attached to it varied. Moreover, since the measured spatial distance between the two functional groups of interest was of ~12 Å, we considered linker lengths ranging from 12-14 atoms. Therefore, the linker size was rationally chosen by determining that the sum of A and B should be always greater or equal to 5 and smaller or equal to 13 (Figure 4).

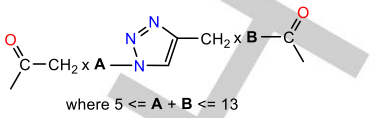


**Figure 4**. Linker design strategy: schematic version of the applied approach followed for the generation of 54 triazole-containing linkers of different lengths.

For the linker screening, the maytansinol and the guanosine molecules were treated as fragments and were fixed in their states seen in the crystal structure 4TV8. Then, we carried out the linker screening and used the docking software S4MPLE[16] to search for the linker that best bridged the gap between the two fragments (maytansinol and guanosine). We observed that none of the generated linkers put any strain on the anchor fragments. Therefore, the linkers were chosen upon synthetic convenience (**a**, Figure 3). We also explored the possibility of designing a more rigid linker by adding a phenyl ring in the side chain of maytansinol. As expected, in this case we observed that the degrees of freedom of the linker were reduced, thus better orienting the linker moiety towards the nucleotide pocket (**b**, Figure 3). We analyzed the validity of the linkers present in conjugates **7** and **8** via template docking. The results showed that both the linkers can flexibly connect both the maytansinol and the guanosine entities in a suitable distance, which allows the two entities to bind tubulin by maintaining a proper geometry.

The interactions established by the nucleotide with β-tubulin were analyzed using computational resources. It was observed that the guanine moiety established the main interactions within the site *via* very specific hydrogen bonds and pi-stacking. Therefore, we also designed conjugate compounds containing acyclovir (**9**, **10**). Docking studies confirmed that the 5-membered ring of the ribose can be substituted without disturbing major interactions of the guanine moiety with β-tubulin. Further, superposition of the docked structure shows that a binding mode resembling the original guanosine one can be adopted (Figure 5). In addition, this choice led to simplifications in the synthesis of maytansinoid-conjugates.

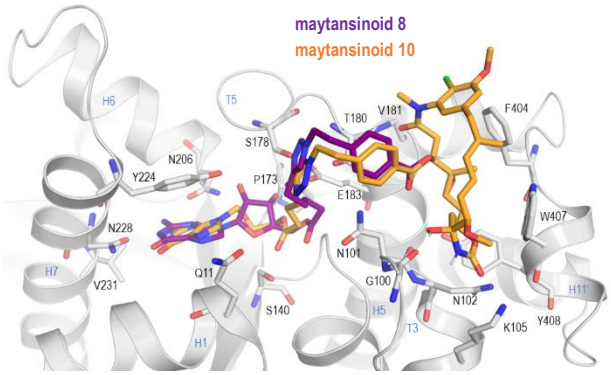


**Figure 5.** Docking result of the maytansinoid-guanosine conjugate **8** (violet) superimposed to the docking result of the maytansinoid-acyclovir conjugate **10** (orange) when bound to tubulin (grey).

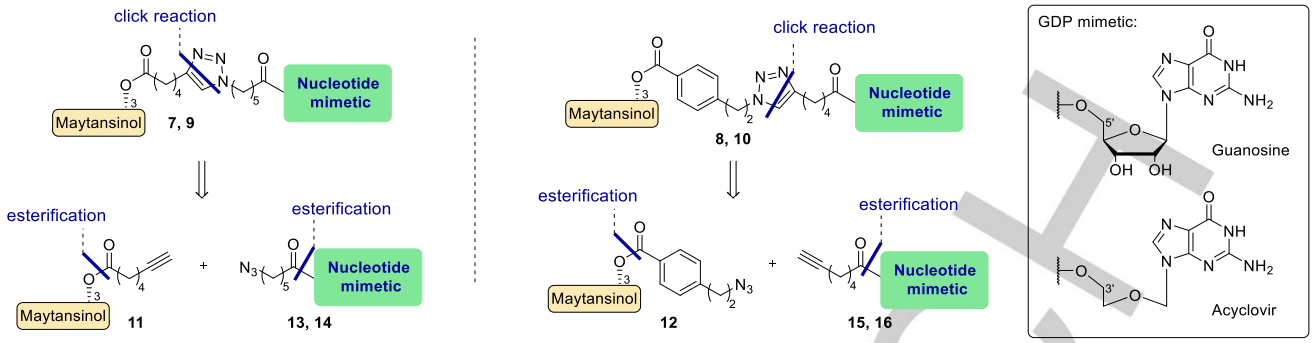


**Scheme 3.** Retrosynthetic pathway of the maytansinoid-conjugates **7-10**.

Conjugate compounds **7-10** can be obtained by a CuAAC reaction between the fragment of an alkyne (**11**, **15**, **16**) and an azide (**12-14**) providing the corresponding triazole derivatives (Scheme 3). Both fragments can be prepared as ester starting from maytansinol and guanosine (or acyclovir) by condensation with carboxylic acids.

Maytansinoids **11** and **12** were obtained using Steglich esterification (Scheme 4) with 6-heptynoic acid or 4-(2-azidoethyl)benzoic acid, which was prepared by treating the corresponding 4-(2-bromoethyl)benzoic acid with $NaN_3$. The yield and selectivity of the acylation reaction can be improved by inhibiting the formations of the undesired maytansinol by-products through the addition of excess $ZnCl_2$, as reported in our previous work.[12]

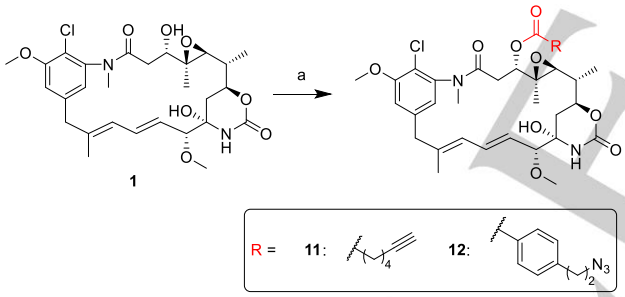


**Scheme 4.** *Reaction conditions*: a) 6-heptynoic acid (or 4-(2-azidoethyl)benzoic acid) 3 equiv., DMAP 3 equiv., DCC 3.3 equiv. in DCM, $ZnCl_2$ 3 equiv., DCM (+10% DMF), 18h (or 24h), **11** 66% (or **12** 68%).

To obtain the nucleotide mimetic fragments **13-16**, 5'-*O*- and 3'-*O*-esterification was performed on guanosine and acyclovir, respectively (Scheme 5). The poor solubility of these compounds in most organic solvents complicates the reactivity and the handling. In this regard, 2',3'-diol or free amine protection of guanosine could be considered.[17–23] However, the isopropylidene ketal formation on guanosine sufficiently increased the solubility, so the $NH_2$ protection was not undertaken. In addition, the formation of the ketal would increase the selectivity for the subsequent 5'-*O* esterification reaction and the formation and removal occur easily under acid condition. Therefore, guanosine was treated with perchloric acid in acetone providing **17** quantitatively.

The literature reports wide reaction conditions useful to perform acylation at 5' position of 2',3'-isopropylidene guanosine, by acyl halides, anhydrides, and acids under coupling conditions.[17,19,24]

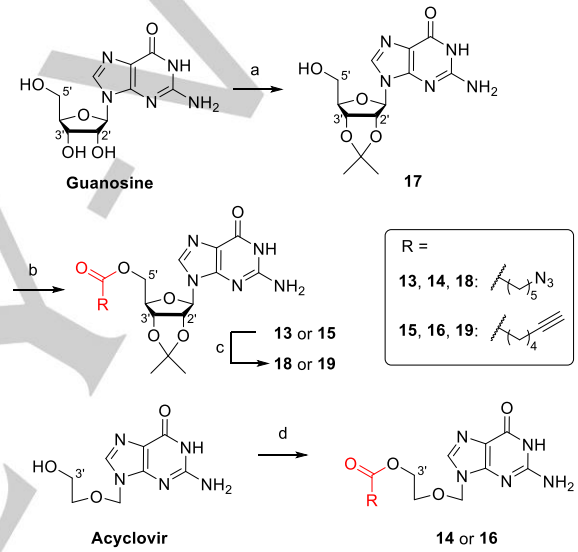


**Scheme 5.** *Reaction conditions*: a) $HClO_4$ 60%, acetone, 18h, quant.; b) 6-azidohexanoic acid (or 6-heptynoic acid) 1.5 equiv., EDC-HCl 1.8 equiv., TEA 2.2 equiv., DMAP 0.6 equiv., DCM, 18h, **13** 71% (or **15** 78%); c) TFA 80% aq, 30 min, **18** 81% (or **19** 98%); d) 6-azidohexanoic acid (or 6-heptynoic acid) 1.5 equiv., EDC-HCl 2.1 equiv., TEA 2.1 equiv., DMAP 0.5 equiv., DCM/DMF 1:1.5, 18h, **14** 64% (or **16** 43%).

The first approach was the coupling of carboxylic acids, therefore compound **17** and acyclovir were similarly esterified with 6-azidohexanoic acid or 6-heptynoic acid in the presence of EDC yielding **13-16**. The reactions on guanosine were performed in DCM giving 71% and 78% in the isolation of the compound **13** and **15** by reverse phase purification, while a mixture of DCM/DMF was used as solvent to overcome the solubility issues of acyclovir obtaining **14** and **16** with a yield of 65% and 43%, respectively.

Considering that deprotection of guanosine in acidic condition could affect the maytansinol part in the final conjugate compounds, the cleavage of isopropylidene was carried out before the click reaction. Therefore, compound **13** and **15** were treated with TFA 80% aq[20,21,24] giving the desired products **18** and **19** with 81% and 98% of yield, respectively.

The alkyne- and azide- building blocks were joined by performing the CuAAC. The reactions carried out on the pairs of

maytansinoid/guanosine **11**/**18** and **12**/**19** with catalytic quantities of $CuSO_4$ in the presence of Na-ascorbate as reducing agent in $H_2O$/*t*-BuOH 1:4 did not lead to any product. The triazole ring was not obtained neither performing the reaction in $H_2O$/DMSO 1:2 as solvent nor by increasing the quantities of the reagents.

In order to better support the solubility of guanosine and the reaction, a new route to carry out the CuAAC was considered. The strategy involved performing the click using the isopropylidene protected guanosine intermediates **13** and **15** and then cleaving the ketal in the final adduct. For this purpose, the experimental conditions to remove protecting group without altering the sensitive structure of maytansinol required a careful condition screening (Table 1).

All conditions except the use of $PdCl_2$ did not affect maytansinol, but at the same time failed to cleave the ketal. Although the use of formic acid with the conditions reported in the literature for the specific removal of acetonide from guanosine produced no results, increasing the acid concentration and heating slightly to 40°C achieved the goal. By $^1$H-NMR analysis the integrity of maytansinol and deprotection of guanosine was confirmed.

**Table 1.** Cleavage conditions of isopropylidene on guanosine in the presence of maytansinol.

| Cleavage Condition | T [°C] | Time [h] | Result |
|---|---|---|---|
| AcOH 80% aq | 25 | 48 | n.r. |
| AcOH 80% aq | 65 | 18 | n.r. |
| $PdCl_2(CH_3CN)_2$ | 60 | 24 | degradation |
| CAN | 25 | 48 | n.r. |
| PPTS | 25 | 48 | n.r. |
| $CuCl_2$-$2H_2O$ | 0 to 25 | 48 | n.r. |
| HCOOH 50% aq [21] | 25 | 48 | n.r. |
| HCOOH 70% aq | 25 | 48 | n.r. |
| HCOOH 70% aq | 40 | 2 | ketal cleavage |

The CuAAC reaction was repeated by treating maytansinoid **11** and protected 5'-*O*-acylguanosine **13** with an excess of $CuSO_4$ and Na-ascorbate in $H_2O$/DMSO 1:2. As expected, the protecting group improved the solubility of guanosine obtaining an excellent result because the triazole ring was formed in few hours with a yield of 89% in the isolation of compound **20**. The same approach was used on **12**/**15** fragment pair to get compound **21** with 85% of yield (Scheme 6).

**Table 2.** Diagnostic $^1$H NMR spectroscopic data of triazole formation *DMSO-d6*.

| Atom | | $^1$H-NMR[a,b] | | $^{13}$C-NMR[a,c] | |
|---|---|---|---|---|---|
| | | from | to | from | to |
| **20** | 33 | 2.28[e] | 2.65 | 18.04[e] | 28.82 |
| | 34 | - | - | 84.20[e] | 146.89 |
| | 35 | 1.95[e] | 7.85 | 69.0[e] | 122.13 |
| | 18G | 3.29 | 4.25 | 51.59 | 49.38 |
| **21** | 35 | 3.70[d] | 4.64 | 52.48[d] | 50.23 |
| | 17G | 2.14 | 2.53 | 18.50 | 25.07 |
| | 18G | - | - | 85.28 | 146.84 |
| | 19G | 2.74 | 7.78 | 72.40 | 121.96 |

[a] Chemical shifts (in ppm) were determined with reference to TMS. [b] Spectra determined at 400 MHz. [c] Spectra determined at 101 MHz. [d] Solvent is *acetone-d6*. [e] Solvent is *chloroform-d.*

The NMR elucidations were completed to confirm the structures, and the shifting of the diagnostic signals demonstrated the formation of triazole on **20** and **21** (Table 2).

Then, both products were treated with formic acid 70% aq at 40°C providing the final conjugate compounds **7** and **8** after 4 hours with yields of 62% and 77%, respectively. The MS and NMR analyses confirmed the isopropylidene deprotection. In case of maytansinoid-acyclovir conjugates, similar conditions were applied using catalytic $CuSO_4$ and Na-ascorbate in $H_2O$/DMF 1:2 as solvent. The desired final products **9** and **10** were obtained in 35% and 55%, respectively (Scheme 7), and fully characterized by NMR and MS analysis (see Supporting Information).

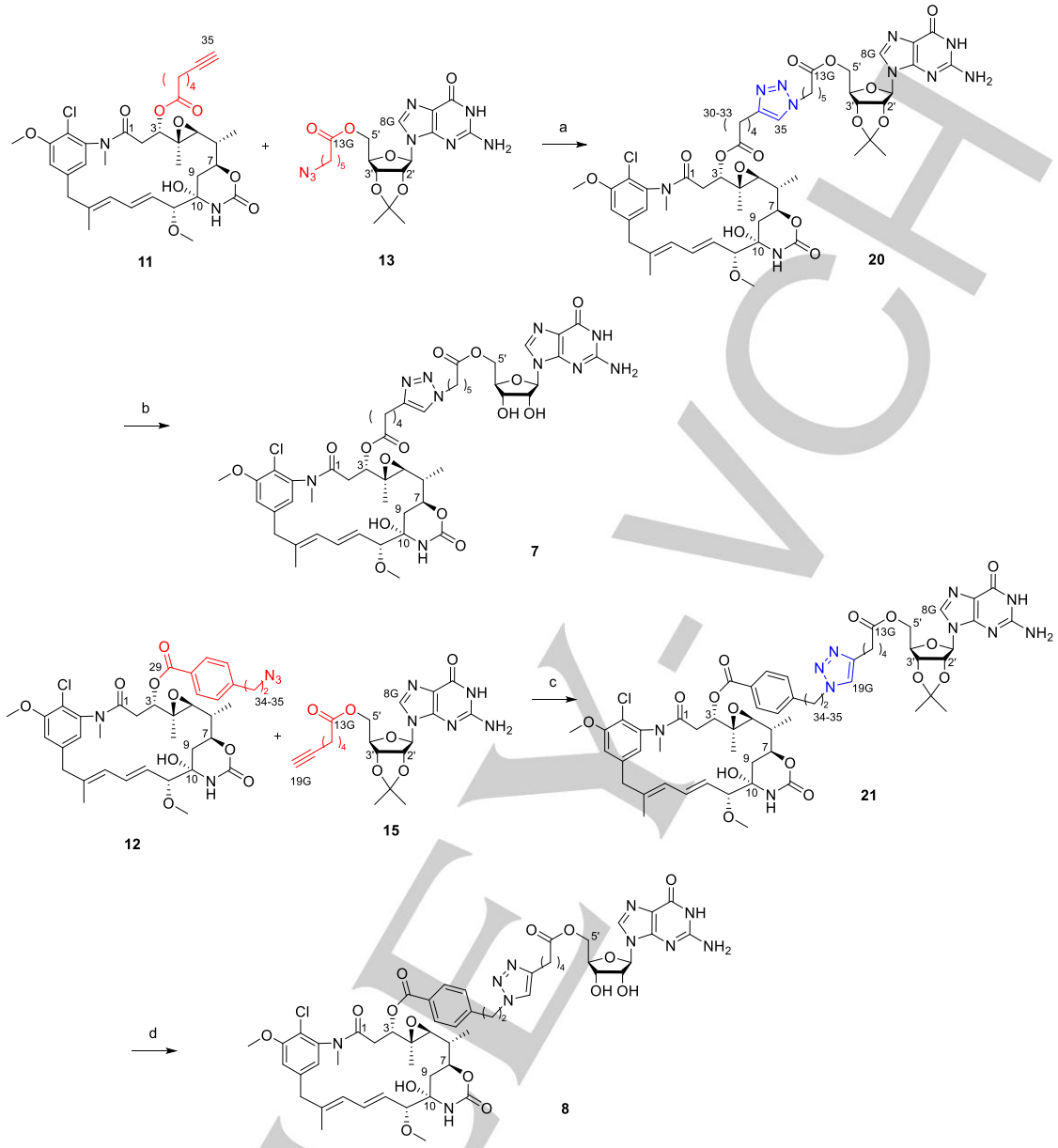


**Scheme 6**. *Reaction conditions*: a) **11** 1 equiv., **13** 1.5 equiv., $CuSO_4$-$5H_2O$ 1.6 equiv., Na-ascorbate 6.4 equiv., $H_2O$/DMSO 1:2, 3h, 89%; b) HCOOH 70% aq, 40°C, 4h, 62%; **c**) **12** 1 equiv., **15** 1.5 equiv., $CuSO_4$-$5H_2O$ 1.6 equiv., Na-ascorbate 6.4 equiv., $H_2O$/DMSO 1:2, 3h, 85%; d) HCOOH 70% aq, 40°C, 4h, 77%.

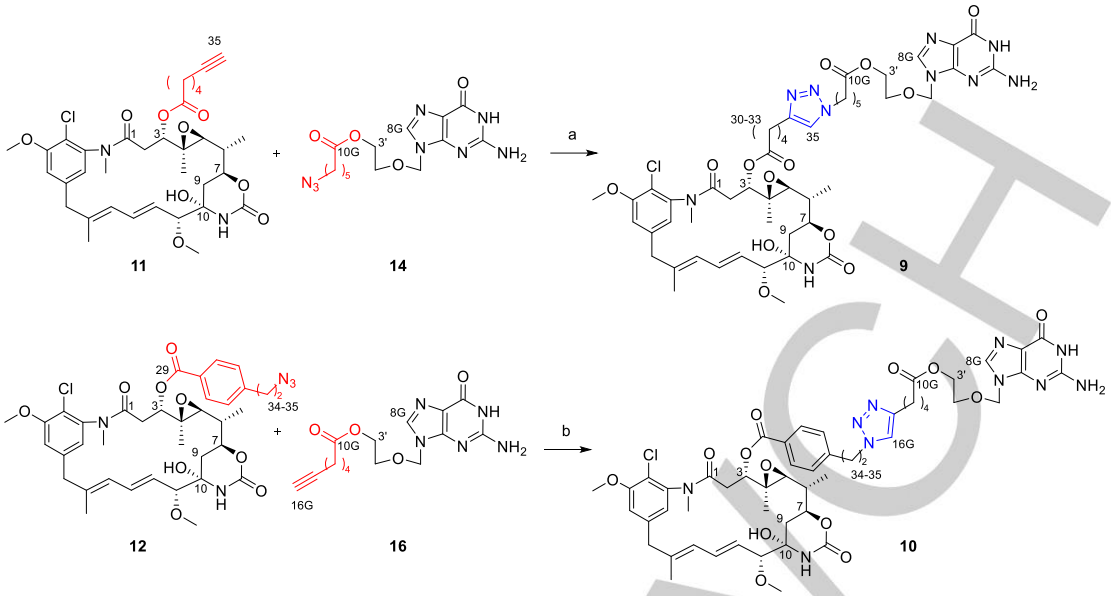


**Scheme 7**. *Reaction conditions*: a) **11** 1 equiv., **14** 1.2 equiv., $CuSO_4$-$5H_2O$ 0.4 equiv., Na-ascorbate 4 equiv., $H_2O$/DMF 1:2, 5h, 35%; b) **12** 1 equiv., **16** 1.2 equiv., $CuSO_4$-$5H_2O$ 0.4 equiv., Na-ascorbate 4 equiv., $H_2O$/DMF 1:2, 6h, 55%.

## Biochemical evaluation

*Inhibition of tubulin assembly*

Maytansine site ligands preclude tubulin assembly by blocking the addition of new tubulin subunits onto the microtubule. Owing to this, we decided to assess the inhibitory effect of this newly synthetized compounds on tubulin polymerization (Figure 6).

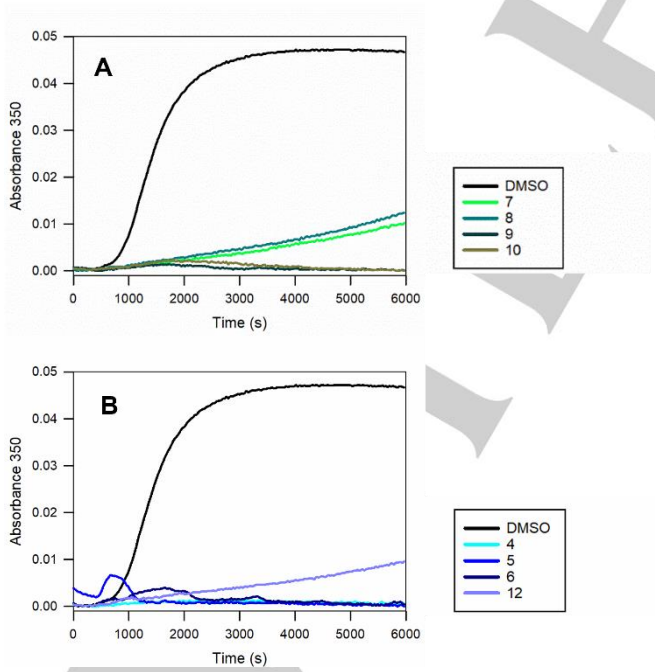


**Figure 6.** Inhibition of tubulin assembly by selected compounds. All experiments were performed as duplicates of two independent experiments. Time courses of assembly of 25 μM tubulin in GAB buffer in the presence of vehicle (DMSO; black lines) or 27.5 μM of **(A)** **7** (light green), **8** (teal), **9** (dark green), 10 (dark yellow); or (**B**) **4** (cyan), **5** (blue), **6** (dark blue), **12** (light purple).

All the compounds analyzed were able to abolish tubulin polymerization.

*Binding affinities*

In order to correlate the tubulin assembly inhibition with the binding affinities of the compounds for the maytansine site, these were determined by means of competition against Fc maytansine (Table 3).[11] Binding affinity is well conserved indicating low or neglectable influence of the side chain in the interaction of the maytansine core with tubulin, but also suggesting little interaction of the nucleotide moiety.

**Table 3**. Binding affinities of maytansinoid compounds[a].

| Compound | Mean Kb ($M^{-1}$) | Kd (nM) |
|---|---|---|
| **maytansine** | $9±1x10^7$ | 11±1 |
| **4** | $9±2x10^6$ | 111±12 |
| **5** | $6±1x10^6$ | 166±24 |
| **6** | $5.3±0.7x10^6$ | 188±22 |
| **7** | $1.2±0.2x10^7$ | 83±12 |
| **8** | $1.3±0.1x10^7$ | 83.4±7.8 |
| **9** | $7.3±0.8x10^6$ | 137±14 |
| **10** | $8±1x10^6$ | 125±14 |
| **11** | $5.4±0.5x10^{7[b]}$ | 19±2[b] |
| **12** | $1.3±0.3x10^7$ | 77±15 |

[a] Data are the mean ± SEM values of three independent experiments with duplicates in each one.[b] Data from Marzullo et al 2022.

*Cytotoxicity*

To correlate the potency of binding with the toxicity, and to investigate the potential of the compounds to overcome membrane pumps mediated multidrug resistance, we determined

the cytotoxicity of the compounds both in A549 and in the isogenic pair A2780/A2780AD (pGp overexpressing) cell lines (Table 4). Consistently with the binding affinity data, compounds **4**, **5**, **6**, **11** and **12** show very good activity against the tumoral cells, being some of them even more active than the parental compound maytansine. On the other hand, compounds containing the triazole moiety arising from the click reaction undergo a severe loss of activity without losing binding affinity, which suggests that the resulting side chain precludes internalization in the cells.

**Table 4**. IC50 of maytansinoid compounds in A549 and A2780/A2780AD cell lines[a].

| Compound | A549 $IC_{50}$ (nM) | A2780 $IC_{50}$ (nM) | A2780AD $IC_{50}$ (nM) | R/S |
|---|---|---|---|---|
| ***Maytansine*** | 0.92±0.07 | 0.26±0.03 | 12±0.4 | 46 |
| ***4*** | 0.26±0.01 | 0.07±0.02 | 11±2 | 157 |
| ***5*** | 0.27±0.01 | 0.37±0.02 | 33±3 | 89 |
| **6** | 4.9±0.3 | 2.0±0.4 | 400±70 | 200 |
| **7** | 11600±700 | 620±50 | 21000±1000 | 34 |
| **8** | 4800±300 | 160±10 | 16000±2000 | 100 |
| **9** | 10.4±0.5 | 4.4±0.5 | 900±100 | 204 |
| ***10*** | 49±3 | 35±4 | 3600±500 | 103 |
| ***11*** | 0.07±0.008[b] | 0.033±0.003[b] | 4.7±0.6[b] | 142 |
| ***12*** | 1.1±0.2 | 0.14±0.01 | 17±3 | 121 |

[a] Data are the mean ± SEM values of three independent experiments with duplicates in each one.[b] Data from Marzullo et al 2022.

### X-ray crystallography structure determination

To evaluate if the attachment of long chains to the maytansine scaffold impacts the binding mode of the molecules, we sought to determine the structures of tubulin-maytansinoid complexes by X-ray crystallography. Crystals of the $T_2$R-TTL complex were grown using our well-established protocols.[25,26] Maytansinoids **4** – **12** were either soaked into the crystals at 5 mM final concentration for 6 - 16 h or added to the crystallization mixture. We collected high resolution data (1.9 Å - 2.6 Å) and used DIMPLE[27] to spot densities of bound ligands.

Consistently with the biochemical data we observed ligand shaped difference density at the maytansine site for all compounds, highlighting that none of the introduced moieties precluded binding in the crystal system. However, only the central ring of the maytansine scaffold was well resolved, while the introduced linkers were not defined in any structure of the obtained maytasinoid-tubulin complexes. These results are in line with the measured binding constants.

The crystal structures of the representative compounds with different side-chain substituents and high cytotoxicity, **4, 6,** and **12**, were further refined to determine their detailed molecular interactions (PDB IDs 8B7A, 8B7B and 8B7C). In general, all three determined structures superposed well with the structure of the parent compound (PDB ID: 4TV8; RMSD of superposition over Ca:0.380 Å (1993 atoms), 0.256 Å (1992 atoms) and 0.330 Å (1982 atoms) for T2R-TTL **4**, **6** and **12** respectively), and there were no major alterations in the binding mode (Figure 7). The insertion of long chains via acylation reaction at the C3-O has no impact on the previously described interactions, namely the hydrogen bonds of the C1 carbonyl to the Val181 main chain nitrogen, the C24 carbonyl to the Lys105 and Asn102 sidechain amine groups and C9-OH to the Gly100 main chain carbonyl. This is as well in line with our previous observation, that insertion of a smaller group at this position has no effect on the binding mode nor on the toxicity of the maytansinoids.[12]

The observed ligand density in these structures extended up to 2-3 carbons beyond the well resolved ester-group linking the chain to the C3 carbon, indicating that the introduced linker-moieties adapt multiple conformations. Accordingly, the carbon chains in all the three structures were modeled and refined in their most probable conformations. Our data highlight the C3-O position as an excellent point to introduce modifications on the maytansine scaffold, allowing the accommodation of long flexible chains or even bulky moieties.

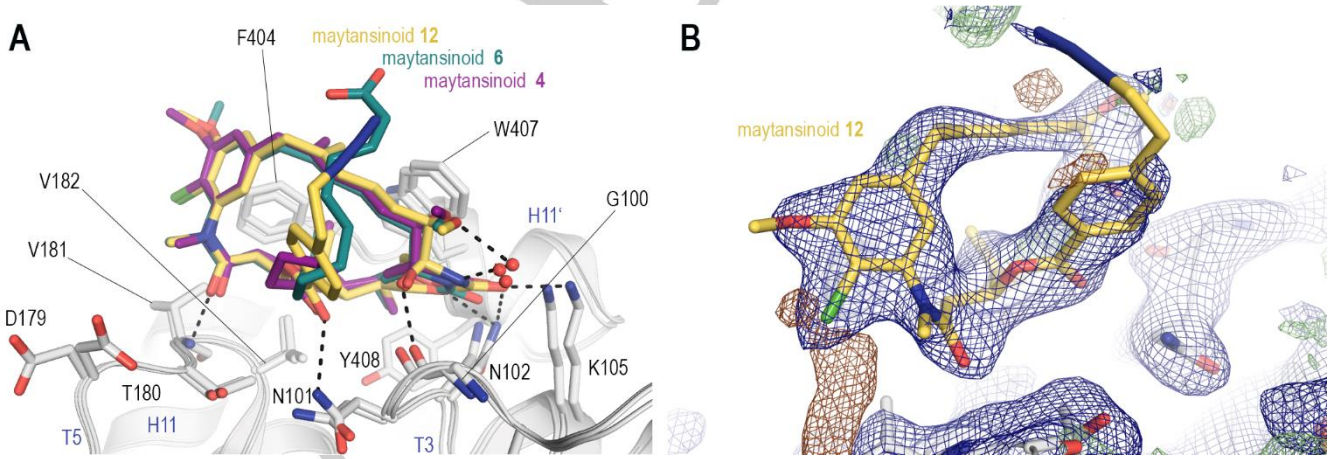


**Figure 7.** Binding poses of maytansinoids **4**, **6** and **12** (PDB IDs: 8B7A, 8B7B, 8B7C) and their fit into the electron density. The molecular interactions of the three superimposed structures of maytansinoids **4** (purple), **6** (cyan) and **12** (yellow) in complex with β-tubulin are displayed in **A**. The protein backbone (grey) is shown in ribbon representation and interacting residues and ligands are shown in sticks. Oxygen, nitrogen and chlorine atoms are colored red, blue and green, respectively, while water molecules are shown as red spheres. All three maytansinoids adopt the same pose as their parent compound maytansine and establish hydrogen bonds to the main chain carbonyl and amide of Gly100 and Val181, respectively, and direct or water-mediated hydrogen bonds to the side chains of Asn101, Asn102 and Lys105 as indicated by the dashed black lines. The long chains attached via esterification of C3-O in **6** and **12** are highly mobile and adopt many different conformations, therefore, there is no defined electron density is visible for these long carbon chains, as shown in panel **B**. The highlighted definition and extension of the electron density to just 2-3 atoms beyond the well-defined C3-ester moiety is representative for all the soaked maytansinoids **4-10** and **12**. The electron density maps 2mFo-DFc (blue mesh) and mFo-DFc (green/red mesh) are contoured at + 1.0 σ and 3.0 σ, respectively.

The lack of defined density and thus a stable conformation of the linker chain showed that compound 6 is not coordinating the Mg2+ ion, since the coordination would result in a fixed position of the carbonic acid linker. Presumably, the exposed nature of the binding site and the high flexibility of the long carbon chains precluded the stable coordination of the $Mg^{2+}$ ion. Moreover, we cannot exclude an additional impact on the interaction by the presence of GDP:$Mg^{2+}$ at the E-site in our crystal system.
Further, we could not observe any evidence for the exchange of the GDP by our nucleotide mimetics neither by soaking nor in co-crystallization experiments. Likely, the very high affinity of nucleotides to tubulin prevents the exchange of the previously bound nucleotide.

## Conclusion

In this work, we have established robust chemistry that allows to place large substituents on a complex natural product. By introducing alkene or alkyne moieties via acylation reaction in position C-3 we opened up the scaffold for the straight-forward attachment of more functional probes. It allows to attach a whole variety of new molecules to the maytansine scaffold by either cross metathesis or click chemistry reactions.

In this work we used these pathways to further investigate the tolerance towards the introduction of bulkier groups and their impact on tubulin binding. Guided by computational studies, we generated a whole set of maytansinoids carrying either long carbon chains, carboxylic acids or nucleotide mimetics. Our compiled data on the inhibition of tubulin assembly and binding affinities, together with the structural information confirms that even these long and heavy groups are tolerated easily. They neither impact the binding mode on tubulin nor dramatically reduce the scaffolds affinity, with even the lowest measured $K_D$ within the nM range. Unexpectedly, the cell permeability is likely affected by the introduction of the larger groups, as observed in their lowered cytotoxicity.

Therefore, our work lays the foundation to further exploit the C3 position of maytansinoids by introducing functional modifications, such as specific fluorophores or chelators, which could potentially serve as probes to study MT dynamics *in vitro*. Furthermore, these modifications could comprise other types of chemical entities for the development of maytansinol-based bivalent compounds capable to recruit specific proteins of interest.

## Experimental Section

**Molecular modeling:** Molecular modeling was applied to test the suitability of the different bulky substituents attached to maytansinol for the generation of long-chain maytansinoids and, to support linker length design and selection for the development of maytansinoid conjugates. The molecular modeling technique used in this paper was molecular docking. To perform the docking experiments the software used was S4MPLE, an in-house developed tool that allowed us to dock the long-chain maytansinoids within the maytansine binding site and its surroundings, and the maytansinoid conjugates within the GTP and maytansine tubulin binding sites and their connecting structural environment.

**Synthesis:** Unless otherwise stated, reagents were purchased from general suppliers (Sigma Aldrich and Fluorochem) and used without further purification. All solvents were of reagent grade or HPLC grade. All reactions were carried out in oven-dried glassware and dry solvents, under nitrogen atmosphere and were monitored by glasses or aluminium TLC on silica gel (Merck precoated 60F254 plates), with detection by UV light (254 nm), or by TLC stains as permanganate, or by HPLC Agilent 1100. Analytical HPLC was performed on Agilent 1100 Series System RP column ZORBAX SB-C8 (3.5µm x 4.6 x 150 mm). The pressure was about 85 bar, with a constant flow rate of 1 mL/min. UV spectra were recorded at 254 nm and 210 nm with DAD detection. The mobile phase consisted of a mixture of $H_2O$/ACN and the gradient was programmed using the following method: isocratic for 1 min at 50% ACN, then gradient for 10 min to 90% ACN. Products were purified using Biotage Isolera™ One System and Biotage® Sfär C18 6 g D¬ Duo 30 µm as cartridges (BIOTAGE).

*General maytansinol acylation procedure for the synthesis of maytansinoids **4**, **5**, **11**,**12**:* To a solution of maytansinol **1** (50 mg, 0.088 mmol, 1 eq) in dry $CH_2Cl_2$ (440 µL) were added DMF dry (44 µL), DMAP (33 mg, 0.26 mmol), the carboxylic acid (0.26 mmol), and $ZnCl_2$ (36 mg, 0.26 mmol) at room temperature under a nitrogen atmosphere. Then, a solution of DCC in dry $CH_2Cl_2$ (60 mg, 0.29 mmol, 1.3 M) was slowly added. The mixture was stirred at room temperature for 48 h before filtering off the DCU using cold $CH_2Cl_2$. The organic phase was washed with $H_2O$ (4 × 1 mL), with brine (1 × 1 mL), then dried over $Na_2SO_4$, and concentrated under reduced pressure. The residue was purified with Biotage Isolera™ One System (gradient $H_2O$/ACN) to provide the desired product as a white powder (Table S1).

*Synthesis of compound **6**:* To a solution of **5** (20 mg, 0.0279 mmol) in dry $CH_2Cl_2$ (1.2 ml) were added acrylic acid (5.0 mg, 0.070 mmol) and Hoveyda-Grubbs 2nd gen. catalyst (2.63 mg, 15 mol%), predissolved in $CH_2Cl_2$ (0.2 ml). The reaction was stirred at reflux (40 °C) for 6h, after which additional catalyst was added (0.88 mg, 5 mol%) and the reaction was stirred overnight. The solvent was evaporated under reduced pressure. The crude was purified with Biotage Isolera™ One System (gradient $H_2O$/ACN) providing the product (9,7 mg, 46%) as a white powder.

*Synthesis of compound **17**:* To a suspension of guanosine (200 mg, 0.706 mmol) in dry acetone (11.8 ml) was added an aqueous solution of 60% $HClO_4$ 60% (95 µL, 0.946 mmol) and the clear reaction obtained was stirred for 2 h at room temperature. The reaction was quenched by dropping an aqueous solution of 28% $NH_4OH$ (134 µL) at 0°C. The precipitate was recovered by filtration on Buchner washing with cold $Et_2O$. The solid was dried in vacuum to provide 229 mg (>98%) of product as white solid.

*Synthesis of compound **13:*** To a solution of **17** (100 mg, 0.309 mmol) in dry $CH_2Cl_2$ (2.5 mL) were added 6-azidohexanoic acid (72 mg, 0.464 mmol), DMAP (22 mg, 0.185 mmol), EDC-HCl (106 mg, 0.557 mmol), and triethylamine dry (95 µL, 0.680 mmol) at room temperature under a nitrogen atmosphere. The reaction was stirred for 18 h before $H_2O$ was added (1 × 2 mL). The organic layer was dried over $Na_2SO_4$, and concentrated under reduced pressure. Purification with Biotage Isolera™ One System (gradient $H_2O$/ACN) provided the product (101 mg, 71%) as a white powder.

*Synthesis of compound **14**:* To a solution of acyclovir (150 mg, 0.666 mmol) in dry $CH_2Cl_2$ (1.0 mL) and dry DMF (1.5 mL) were added 6-azidohexanoic acid (158 mg, 1.006 mmol), DMAP (41 mg, 0.336 mmol), EDC-HCl (269 mg, 1.405 mmol), and triethylamine dry (196 µL, 1.405 mmol) at room temperature

under a nitrogen atmosphere. The reaction was stirred overnight. Then, the solvent was removed under reduced pressure. The crude was purified with Biotage Isolera™ One System (gradient $H_2O$/ACN), providing the product (154,8 mg, 65%) as a white powder.

*Synthesis of compound **15**:* To a solution of **17** (150 mg, 0.464 mmol) in dry $CH_2Cl_2$ (3.8 mL) were added 6-heptynoic acid (88 µL, 0.696 mmol), DMAP (34 mg, 0.278 mmol), EDC-HCl (160 mg, 0.835 mmol), and triethylamine dry (142 µL, 1.021 mmol) at room temperature under a nitrogen atmosphere. The reaction was stirred for 18 h before $H_2O$ was added (1 × 3 mL). The organic layer was dried over $Na_2SO_4$, and concentrated under reduced pressure. Purification with Biotage Isolera™ One System (gradient $H_2O$/ACN) provided the product (156 mg, 78%) as a white powder.

*Synthesis of compound **16**:* To a solution of acyclovir (150 mg, 0.666 mmol) in dry $CH_2Cl_2$ (1.25 mL) and dry DMF (1.25 mL) were added 6-heptynoic acid (135 mg, 1.07 mmol), DMAP (41mg, 0.336 mmol), EDC-HCl (269 mg, 1.405 mmol), and triethylamine dry (196 µL, 1.405 mmol) at room temperature under a nitrogen atmosphere. The reaction was stirred overnight. The crude was purified with Biotage Isolera™ One System (gradient $H_2O$/ACN), providing the product (95,5 mg, 43%) as a white powder.

*Synthesis of compound **18**:* To a solution of **13** (49 mg, 0.11 mmol) was added aqueous TFA 80% (1.52 mL). The mixture was stirred at room temperature for 30 min. Then, the solvent was removed in vacuum, a solution of EtOH +1% $Et_3N$ (2.5 mL) were added and the solvent was evaporated to remove the TFA salt form. Purification of the crude with Biotage Isolera™ One System (gradient $H_2O$/ACN) provided the product (46 mg, >98%) as a white powder.

*Synthesis of compound **19**:* To a solution of **15** (52 mg, 0.12 mmol) was added aqueous TFA 80% (1.71 mL). The mixture was stirred at room temperature for 30 min. Then, the solvent was removed in vacuum, a solution of EtOH +1% $Et_3N$ (2.5 mL) were added and the solvent was evaporated to remove the TFA salt form. Purification of the crude with Biotage Isolera™ One System (gradient $H_2O$/ACN) provided the product (46 mg, >98%) as a white powder.

*Synthesis of compound **20**:* To a solution of **11** (21 mg, 0.031mmol) and **13** (21 mg, 0.047 mmol) in DMSO (690 µL) were added water (225 µL), CuSO4*5$H_2O$ (15 mg, 0.050 mmol), then a solution of Na-ascorbate (39 mg, 0.19 mmol) in H2O (115 µL) was added dropwise. The mixture was stirred at room temperature for 2 h. Then, water was added (1.4 mL) and the aqueous layer was extracted in DCM. The organic layer was washed with $H_2O$ and brine, dried over $Na_2SO_4$ and concentrated in vacuum. Purification of the crude with Biotage Isolera™ One System (gradient $H_2O$/ACN) provided the product (31 mg, 89%) as a white powder.

*Synthesis of compound **21**:* To a solution of **12** (16 mg, 0.022 mmol) and **15** (14 mg, 0.032 mmol) in DMSO (482 µL) were added water (159 µL), $CuSO_4$*5$H_2O$ (10 mg, 0.035 mmol), then a solution of Na-ascorbate (28 mg, 0.139 mmol) in $H_2O$ (82 µL) was added dropwise. The mixture was stirred at room temperature for 2 h. Then, water was added (1.4 mL) and the aqueous layer was extracted in DCM. The organic layer was washed with $H_2O$ and brine, dried over $Na_2SO_4$ and concentrated in vacuum. Purification of the crude with Biotage Isolera™ One System (gradient $H_2O$/ACN) provided the product (22 mg, 85%) as a white powder.

*Synthesis of compound **7**:* To compound **20** (18.3 mg, 0.016 mmol) was added aq. 70% HCOOH (650 µL) and the reaction was stirred for 4 hours at 40°C. Then, the solvent was removed under reduced pressure and the acid was co-evaporated by adding and evaporating three times MeOH. Purification of the crude with Biotage Isolera™ One System (gradient $H_2O$/ACN) provided the product (11 mg, 62%) as a white powder.

*Synthesis of compound **8**:* To compound **21** (11 mg, 0.009 mmol) was added aq. 70% HCOOH (235 µL) and the reaction was stirred for 4 hours at 40°C. Then, the solvent was removed under reduced pressure and the acid was co-evaporated by adding and evaporating three times MeOH. Purification of the crude with Biotage Isolera™ One System (gradient $H_2O$/ACN) provided the product (8 mg, 77%) as a white powder.

*Synthesis of compound **9**:* To a solution of **12** (14 mg, 0.02 mmol) and **14** (9.1 mg, 0.025 mmol) in $H_2O$/DMF as solvents (1:2, 400 µL) were added a solution of $CuSO_4$*5$H_2O$ (11.2 µL of 0.75 M solution, 0.084 mmol), and a solution of Na-ascorbate (83.9 µL of 1M solution, 0.0084 mmol). The mixture was stirred at room temperature for 6h. Crude was purified with Biotage Isolera™ One System (gradient $H_2O$/ACN), providing the product (7 mg, 35%) as a white powder.

*Synthesis of compound **10**:* To a solution of **11** (11 mg, 0.015 mmol) and **16** (6 mg, 0.018 mmol) in $H_2O$/DMF as solvents (1:2, 300 µL) were added a solution of $CuSO_4$*5$H_2O$ (8 µL of 0.75 M solution, 0.06 mmol), and a solution of Na-ascorbate (60 µL of 1M solution, 0.006 mmol). The mixture was stirred at room temperature for 5h. Crude was purified with Biotage Isolera™ One System (gradient $H_2O$/ACN), providing the product (8.8 mg, 55%) as a white powder.

$^1$H NMR and $^{13}$C-NMR spectra were recorded on a Bruker Avance Spectrometer 400 MHz using commercially available deuterated solvents (chloroform-d, methanol-d4, acetone-d6, DMSO-d6, dichloromethane-d2) at room temperature.

$^1$H NMR and $^{13}$C-NMR data for all the synthesized compounds is presented in the Supporting Information.

High resolution mass spectra (HR-MS) were recorded on a Water QToF Premier high resolution UPLC ES MS/MS. Data is included in the Supporting Information.

**Biochemical evaluation:**

*Protein and chemicals for biochemistry*

Calf brain tubulin was obtained by means of a modification of the Weisenberg procedure.[28] Briefly, calf brains were blended prior to perform two salting out steps with ammonium sulfate. Then, a DEAE chromatography was carried out to obtain a 99% pure tubulin. Additionally, a gel filtration chromatography was done to remove all the excess of ammonium sulphate. Finally, tubulin was collected and quantified prior to its liophilization in trehalose buffer and storage at -80.[29]

*Biochemistry*

Polymerization of 25 µM Tubulin in GAB buffer (3.4 M Glycerol, 10 mM sodium phosphate (NaPi), 1 mM EGTA, 6 mM $MgCl_2$, 1 mM GTP, pH 6.7) was monitored in the presence of the desired concentration of the ligand by measuring turbidity at 350 nm employing a Thermo Appliskan plate reader (Thermo Fisher,

Waltham, MA, USA). Data for the polymerization assays were obtained in duplicates of two independent experiments.

Binding constants of the compounds to the maytansine site of tubulin were measured by competition with FcMaytansine as described.[11]DMSO was used as vehicle for maytansine derivatives where less than 0.5% was employed. Data are the mean ± SEM values of three independent experiments with duplicates in each one.

*Cell Biology*

Human A549 non-small lung carcinoma cells, human ovarian carcinomas A2780 and A2780AD (MDR overexpressing P-glycoprotein) were cultured at 37ºC in Dulbecco's Modified Eagle Medium (DMEM) supplemented with 10% fetal calf serum, 2 mM L-glutamine, 1 mM sodium pyruvate, 40 µg/ml gentamycin, 100 IU/ml penicillin and 100 µg/ml streptomycin in a 5% $CO_2$ air atmosphere. Antiproliferation assays were performed as described.[30]DMSO was used as vehicle for maytansine derivatives where less than 0.5% was employed in the assay. Data are the mean ± SEM values of three independent experiments with duplicates in each one. The statistical significance of differences in IC50 values were evaluated using the t-test option implemented in the Sigma Plot software package (version 14.5, Systat Software, Inc., San Jose, CA, USA).

**X-ray crystallography structure determination:**

$T_2$R-TTL crystals were prepared as previously described[25,26,31] and soaked with compounds **4**-**12*** at a final concentration of 5 mM for 6 – 16 h. Crystals were grown at room temperature over one week in buffer containing PEG 4K (5%), glycerol (8%), $MgCl_2$ (30 mM), $CaCl_2$ (30 mM), MES/imidazole pH 6.5 (100mM) and tyrosine (5 mM). X-ray diffraction data were collected at 1 Å wavelength and 100 K at the beamline X06DA of the Swiss Light Source, Paul Scherrer Institut, 5332 Villigen PSI, Switzerland. Datasets were processed using XDS[32] and structures were determined by the difference Fourier method based on phases of a $T_2$R-TTL model in the absence of ligands (PBD ID: 5LXT). Refinement and model building were done in iterative cycles of restrained refinement in PHENIX[33] and model building in Coot.[34] The ligand structures were energy minimized in Moloc[35], before restraint generation with eLBOW (part of the PHENIX suite) and AceDRG[36] in CCP4i2.[37] The quality of the obtained models was monitored with MolProbity.[38] The structures of the $T_2$R-TTL – **4**, **6** and **12** complexes were refined to resolution of 2.25 Å, 2.25 Å and 1.90 Å with crystallographic Rwork / Rfree values of 18.04 / 22.31 %, 18.03 / 22.33 % and 18.52 / 21.93 %, respectively. The detailed statistics for each structure are available in the Supporting Information (Table S2). Coordinates and structure factors were deposited in the PDB with the following accession codes 8B7A, 8B7B and 8B7C. The shown molecular graphics were generated using PyMol (the PyMOL Molecular Graphics System Version 2.3.4 Schrödinger, LLC).

*tubulin-maytansinoid-complex - **11** was previously described[12] (PDB ID: 5SBB)

## Acknowledgements

We thank Ganadería Fernando Díaz for calf brains. We thank the staff of the Swiss Light Source responsible for beamline X06DA for their support during X-ray data collection. This work was supported by the H2020-MSCA-ITN-2019 (860070 TUBINTRAIN), Ministerio de Ciencia e Innovación PID2019-104545RB-I00 (JFD), Proyecto de Investigación en Neurociencia Fundación Tatiana Pérez de Guzmán el Bueno 2020, and by the European Union NextGenerationEU (J.F.D.). Open Access Funding provided by $INSTITUTION within the CRUI-CARE Agreement.

**Keywords:** • chemical probes • maytansinoids • maytansinol functionalization • microtubules • tubulin

[1] S. M. Kupchan, Y. Komoda, W. A. Court, G. J. Thomas, R. M. Smith, A. Karim, C. J. Gilmore, R. C. Haitiwanger, R. F. Bryan, *J. Am. Chem. Soc.* **1972**, *94*, 1354–1356.

[2] S. M. Kupchan, Y. Komoda, A. R. Branfman, A. T. Sneden, W. A. Court, G. J. Thomas, H. P. J. Hintz, R. M. Smith, A. Karim, G. A. Howie, A. K. Verma, Y. Nagao, R. G. Dailey, V. A. Zimmerly, W. C. Sumner, *J. Org. Chem.* **1977**, *42*, 2349–2357.

[3] S. Ikeyama, M. Takeuchi, *Biochem. Pharmacol.* **1981**, *30*, 2421–2425.

[4] A. E. Prota, K. Bargsten, J. F. Diaz, M. Marsh, C. Cuevas, M. Liniger, C. Neuhaus, J. M. Andreu, K. H. Altmann, M. O. Steinmetz, *Proc. Natl. Acad. Sci. U. S. A.* **2014**, *111*, 13817–21.

[5] S. Wedam, L. Fashoyin-Aje, X. Gao, E. Bloomquist, S. Tang, R. Sridhara, K. B. Goldberg, B. L. King-Kallimanis, M. R. Theoret, A. Ibrahim, L. Amiri-Kordestani, R. Pazdur, J. A. Beaver, *Clin. Cancer Res.* **2020**, *26*, 4180–4185.

[6] B. T. Li, R. Shen, D. Buonocore, Z. T. Olah, A. Ni, M. S. Ginsberg, G. A. Ulaner, M. Offin, D. Feldman, T. Hembrough, F. Cecchi, S. Schwartz, N. Pavlakis, S. Clarke, H. H. Won, E. B. Brzostowski, G. J. Riely, D. B. Solit, D. M. Hyman, A. Drilon, C. M. Rudin, M. F. Berger, J. Baselga, M. Scaltriti, M. E. Arcila, M. G. Kris, *J. Clin. Oncol.* **2018**, *36*, 2532–2537.

[7] J. I. Geller, J. G. Pressey, M. A. Smith, R. A. Kudgus, M. Cajaiba, J. M. Reid, D. Hall, D. A. Barkauskas, S. D. Voss, S. Y. Cho, S. L. Berg, J. S. Dome, E. Fox, B. J. Weigel, *Cancer* **2020**, 5303–5310.

[8] S. J. M. Hale, R. D. Perrins, C. E. Garcĺa, A. Pace, U. Peral, K. R. Patel, A. Robinson, P. Williams, Y. Ding, G. Saito, M. Á. Rodriguez, I. Perera, A. Barrientos, K. Conlon, S. Damment, J. Porter, T. Coulter, *Bioconjug. Chem.* **2019**, *30*, 703–713.

[9] J. Porter, Y. Ding, S. J. M. Hale, R. D. Perrins, A. Robinson, M. P. Mazanetz, Y. Wu, Y. Ma, K. Conlon, T. Coulter, *Bioorganic Med. Chem. Lett.* **2020**, *30*, 127634.

[10] C.-F. Lo, T.-Y. Chiu, Y.-T. Liu, P.-Y. Pan, K.-L. Liu, C.-Y. Hsu, M.-Y. Fang, Y.-C. Huang, T.-K. Yeh, T.-A. Hsu, C.-T. Chen, L.-R. Huang, L. K. Tsou, *J. Med. Chem.* **2022**, *65*, 12802–12824.

[11] G. Menchon, A. E. Prota, D. Lucena-Agell, P. Bucher, R. Jansen, H. Irschik, R. Müller, I. Paterson, J. F. Díaz, K. H. Altmann, M. O. Steinmetz, *Nat. Commun.* **2018**, *9*, 2106.

[12] P. Marzullo, Z. Boiarska, H. Pérez-Peña, A. C. Abel, B. Álvarez-Bernad, D. Lucena-Agell, F. Vasile, M. Sironi, K. H. Altmann, A. E. Prota, J. F. Díaz, S. Pieraccini, D. Passarella, *Chem. - A Eur. J.* **2022**, *28*, e202103520.

[13] T. W. Yu, H. G. Floss, in *Anticancer Agents from Nat. Prod. (Ed. Gordon M. Cragg, David G. I. Kingston, David J. Newman)*, CRC Press, Boca Raton, **2005**, p. 321.

[14] W. Li, M. Huang, Y. Li, A. Xia, L. Tan, Z. Zhang, Y. Wang, J. Yang, *Biochem. Biophys. Res. Commun.* **2021**, *566*, 197–203.

[15] T. W. Traut, *Mol. Cell. Biochem.* **1994**, *140*, 1–22.

[16] L. Hoffer, C. Chira, G. Marcou, A. Varnek, D. Horvath, *Molecules*

**2015**, *20*, 8997–9028.

[17] S. Vertuani, A. Baldisserotto, K. Varani, P. A. Borea, B. De Marcos Maria Cruz, L. Ferraro, S. Manfredini, A. Dalpiaz, *Eur. J. Med. Chem.* **2012**, *54*, 202–209.

[18] Y. Pavan Kumar, P. Saha, D. Saha, I. Bessi, H. Schwalbe, S. Chowdhury, J. Dash, *ChemBioChem* **2016**, *17*, 388–393.

[19] J. Camacho-García, C. Montoro-García, A. M. López-Pérez, N. Bilbao, S. Romero-Pérez, D. González-Rodríguez, *Org. Biomol. Chem.* **2015**, *13*, 4506–4513.

[20] Y. Xu, H. Jin, Z. Yang, L. Zhang, L. Zhang, *Tetrahedron* **2009**, *65*, 5228–5239.

[21] B. Zhang, Z. Cui, L. Sun, *Org. Lett.* **2001**, *3*, 275–278.

[22] R. Shah, A. Strom, A. Zhou, K. M. Maize, B. C. Finzel, C. R. Wagner, *ACS Med. Chem. Lett.* **2016**, *7*, 780–784.

[23] S. Vincent, S. Grenier, A. Valleix, C. Salesse, L. Lebeau, C. Mioskowski, *J. Org. Chem.* **1998**, *63*, 7244–7257.

[24] Y. Xiong, J. Lu, J. Hunter, L. Li, D. Scott, H. G. Choi, S. M. Lim, A. Manandhar, S. Gondi, T. Sim, K. D. Westover, N. S. Gray, *ACS Med. Chem. Lett.* **2017**, *8*, 61–66.

[25] M. O. S. T. Muhlethaler, N. Olieric, V.A. Ehrhard, M. Wranik, J. Standfuss, A. Sharma, A.E. Prota, in *Methods Mol. Biol. Humana, New York,* **2022**, pp. 349–374.

[26] A. E. Prota, K. Bargsten, D. Zurwerra, J. J. Field, J. F. Díaz, K. H. Altmann, M. O. Steinmetz, *Science (80-. ).* **2013**, *339*, 587–590.

[27] M. Wojdyr, R. Keegan, G. Winter, A. Ashton, *Acta Crystallogr. Sect. A Found. Crystallogr.* **2013**, *69*, 299.

[28] J. M. Andreu, in *Methods Mol. Biol. Vol. 137 (Ed J. Zhou) Ch. Microtubule Protoc.*, Humana Press Inc., **2007**, pp. 17–28.

[29] E. Dráberová, V. Sulimenko, T. Sulimenko, K. J. Böhm, P. Dráber, *Anal. Biochem.* **2010**, *397*, 67–72.

[30] R. M. Buey, I. Barasoain, E. Jackson, A. Meyer, P. Giannakakou, I. Paterson, S. Mooberry, J. M. Andreu, J. F. Díaz, *Chem. Biol.* **2005**, *12*, 1269–1279.

[31] A. E. Prota, M. M. Magiera, M. Kuijpers, K. Bargsten, D. Frey, M. Wieser, R. Jaussi, C. C. Hoogenraad, R. A. Kammerer, C. Janke, M. O. Steinmetz, *J. Cell Biol.* **2013**, *200*, 259–270.

[32] W. Kabsch, *Acta Crystallogr. Sect. D Biol. Crystallogr.* **2010**, *66*, 125–132.

[33] P. D. Adams, P. V. Afonine, G. Bunkóczi, V. B. Chen, I. W. Davis, N. Echols, J. J. Headd, L. W. Hung, G. J. Kapral, R. W. Grosse-Kunstleve, A. J. McCoy, N. W. Moriarty, R. Oeffner, R. J. Read, D. C. Richardson, J. S. Richardson, T. C. Terwilliger, P. H. Zwart, *Acta Crystallogr. Sect. D Biol. Crystallogr.* **2010**, *66*, 213–221.

[34] P. Emsley, B. Lohkamp, W. G. Scott, K. Cowtan, *Acta Crystallogr. Sect. D Biol. Crystallogr.* **2010**, *66*, 486–501.

[35] P. R. Gerber, K. Müller, *J. Comput. Aided. Mol. Des.* **1995**, *9*, 251–268.

[36] F. Long, R. A. Nicholls, P. Emsley, S. Gražulis, A. Merkys, A. Vaitkus, G. N. Murshudov, *Acta Crystallogr. Sect. D Struct. Biol.* **2017**, *73*, 112–122.

[37] L. Potterton, J. Agirre, C. Ballard, K. Cowtan, E. Dodson, P. R. Evans, H. T. Jenkins, R. Keegan, E. Krissinel, K. Stevenson, A. Lebedev, S. J. McNicholas, R. A. Nicholls, M. Noble, N. S. Pannu, C. Roth, G. Sheldrick, P. Skubak, J. Turkenburg, V. Uski, F. Von Delft, D. Waterman, K. Wilson, M. Winn, M. Wojdyr, *Acta Crystallogr. Sect. D Struct. Biol.* **2018**, *74*, 68–84.

[38] I. W. Davis, L. W. Murray, J. S. Richardson, D. C. Richardson, *Nucleic Acids Res.* **2004**, *32*, W615-619.

## Entry for the Table of Contents

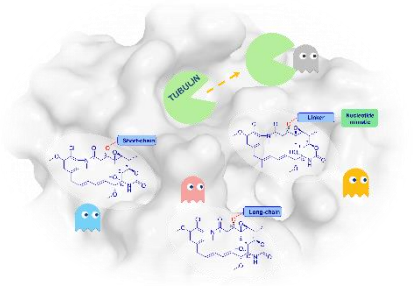


Design, synthesis, biochemical and structural characterization of long-chain maytansinoids and maytansinoid conjugates is reported. The obtained results show the prospects of maytansinoids as probes to study microtubules dynamics and lead towards the design of new maytansine-based derivatives.